

1 **The Epstein-Barr virus ubiquitin deconjugase BPLF1 regulates the activity**  
2 **of Topoisomerase II during virus replication**

3  
4  
5  
6

7 Jinlin Li<sup>1,4</sup> Noemi Nagy<sup>1</sup>, Jiangnan Liu<sup>1</sup>, Soham Gupta<sup>1,5</sup>, Teresa Frisan<sup>2</sup> Thomas Hennig<sup>3</sup>,  
8 Donald P. Cameron<sup>1</sup>, Laura Baranello<sup>1</sup>, and Maria G. Masucci<sup>1§</sup>

9 <sup>1</sup>Department of Cell and Molecular Biology, Karolinska Institutet, S-17165, Stockholm,  
10 Sweden

11 <sup>2</sup>Department of Molecular Biology, Umeå Center for Microbial Research, Umeå University, S-  
12 90187 Umeå, Sweden

13 <sup>3</sup>Institute for Virology and Immunobiology, University of Würzburg, 97078 Würzburg,  
14 Germany

15 <sup>4</sup>Current address: Institute of Medical Biochemistry and Microbiology, Uppsala University, S-  
16 75121, Uppsala, Sweden

17 <sup>5</sup>Current address: Division of Clinical Microbiology, Department of Laboratory Medicine  
18 Karolinska Institutet, S-14152, Huddinge, Sweden.

19  
20  
21

22 Short title: Regulation of Topoisomerase-II by BPLF1

23  
24  
25  
26

§ Corresponding author: Maria G. Masucci, CMB, Biomedicum A6, Karolinska Institutet, S-  
17165, Stockholm, Sweden; e-post: maria.masucci@ki.se

27 **Abstract**

28 Topoisomerases are essential for the replication of herpesviruses but the mechanisms by which  
29 the viruses hijack the cellular enzymes are largely unknown. We found that topoisomerase-II  
30 (TOP2) is a substrate of the Epstein-Barr virus (EBV) ubiquitin deconjugase BPLF1. BPLF1  
31 selectively inhibited the ubiquitination of TOP2 following treatment with topoisomerase  
32 poisons, interacted with TOP2 $\alpha$  and TOP2 $\beta$  in co-immunoprecipitation and *in vitro* pull-down,  
33 stabilized Etoposide-trapped TOP2 cleavage complexes (TOP2cc) and promoted TOP2  
34 SUMOylation, which halted the DNA-damage response and reduced Etoposide toxicity.  
35 Induction of the productive virus cycle promoted the accumulation of TOP2 $\beta$ cc, enhanced  
36 TOP2 $\beta$  SUMOylation, and reduced Etoposide toxicity in lymphoblastoid cell lines carrying  
37 recombinant EBV encoding the active enzyme. Attenuation of this phenotype upon expression  
38 of a catalytic mutant BPLF1-C61A impaired viral DNA synthesis and virus release. These  
39 findings highlight a previously unrecognized function of BPLF1 in promoting non-proteolytic  
40 pathways for TOP2cc debulking that favor cell survival and virus production.

41

42

## 43 **Introduction**

44 Epstein–Barr virus (EBV) is a human gamma-herpesvirus that establishes life-long persistent  
45 infections in most adults worldwide. The virus has been implicated in the pathogenesis of a  
46 broad spectrum of diseases ranging from infectious mononucleosis (IM) to a variety of  
47 lymphoid and epithelial cell malignancies including both Hodgkin and non-Hodgkin  
48 lymphomas, undifferentiated nasopharyngeal carcinoma, and gastric cancer(Shannon-Lowe &  
49 Rickinson, 2019).

50 Like other herpesviruses, EBV establishes latent or productive infections in different cell types.  
51 In latency, few viral genes are expressed resulting in the production of proteins and non-coding  
52 RNAs that drive virus persistence and cell proliferation(Babcock et al., 1998). In contrast,  
53 productive infection requires the coordinated expression of a large number of immediate early,  
54 early and late viral genes, which leads to the assembly of progeny virus and death of the infected  
55 cells(Hammerschmidt & Sugden, 2013). Although much of the EBV-induced pathology has  
56 been attributed to viral latency, the importance of lytic products in the induction of chronic  
57 inflammation and malignant transformation is increasingly recognized(Munz, 2019), pointing  
58 to inhibition of virus replication as a useful strategy for preventing EBV associated diseases.

59 EBV replication is triggered by the expression of immediate early genes, which  
60 transcriptionally activates a variety of viral and host cell factors required for subsequent phases  
61 of the productive cycle(Countryman & Miller, 1985; Feederle et al., 2000; Murata, 2014).  
62 Among the cellular factors, DNA topoisomerase-I and -II (TOP1 and TOP2) were shown to be  
63 essential for herpesvirus DNA replication(Hammarsten et al., 1996; M Kawanishi, 1993; Wang  
64 et al., 2008), raising the possibility that topoisomerase inhibitors may serve as antivirals. Indeed,  
65 non-toxic concentrations of TOP1 and TOP2 inhibitors were shown to suppress EBV-DNA  
66 replication(M Kawanishi, 1993), and different TOP1 inhibitors reduced the transcriptional

67 activity of the EBV immediate-early protein BZLF1 and the assembly of viral replication  
68 complexes(Wang et al., 2009). However, the mechanisms by which the virus harnesses the  
69 activity of these essential cellular enzymes remain largely unknown.

70 Topoisomerases sustain DNA replication, recombination and transcription by inducing  
71 transient single or double-strand DNA breaks that allow the resolution of topological problems  
72 arising from strand separation(Champoux, 2001; Wang, 2002). TOP2 homodimers mediate  
73 DNA disentanglement by inducing transient double strand-breaks (DSBs) through the  
74 formation of enzyme-DNA adducts, known as TOP2 cleavage complexes (TOP2ccs), between  
75 catalytic tyrosine residues and the 5'ends of the DSBs(Nitiss, 2009). Following the passage of  
76 the second DNA strand, TOP2 rejoins the DNA ends via reversion of the trans-esterification  
77 reaction. While TOP2-induced DSBs are relatively frequent in genomic DNA(Morimoto et al.,  
78 2019), failure to resolve TOP2ccs, as may occur upon endogenous or chemical stress that  
79 inhibits TOP2 activity, results in the formation of stable TOP2-DNA adducts that hinder DNA  
80 replication and transcription and trigger apoptotic cell death(Kaufmann, 1998). Thus, cellular  
81 defense mechanisms attempt to resolve the TOP2ccs via proteolytic or non-proteolytic  
82 mechanisms(Sun, Saha, et al., 2020). These may involve the displacement of TOP2 via  
83 ubiquitin(Mao et al., 2001) or SUMO and ubiquitin-dependent(Sun, Miller Jenkins, et al., 2020)  
84 proteasomal degradation, which, following the removal of residual peptide-DNA adducts by  
85 the Tyrosyl-DNA phosphodiesterase-2 (TDP2) resolving enzyme(Gao et al., 2014; Pommier et  
86 al., 2014), unmasks the DNA breaks and promotes activation of the DNA damage response  
87 (DDR)(Pommier et al., 2014). Alternatively, SUMOylation may induce conformational  
88 changes in the TOP2 dimer the expose the covalent bonds to the direct action of  
89 TDP2(Schellenberg et al., 2017). Two TOP2 isozymes expressed in mammalian cells share  
90 ~70% sequence identity and have similar catalytic activities and structural features but are  
91 differentially regulated and play distinct roles in biological processes(Nitiss, 2009). While

92 TOP2 $\alpha$  is preferentially expressed in dividing cells and is essential for decatenating intertwined  
93 sister chromatids during mitosis(Chen et al., 2015), TOP2 $\beta$  is the only topoisomerase expressed  
94 in non-proliferating cells and is indispensable for transcription(Madabhushi, 2018)-(McKinnon,  
95 2016).

96 Ubiquitin-specific proteases, or deubiquitinating enzymes (DUBs), regulate protein turnover by  
97 disassembling poly-ubiquitin chains that target the substrate for proteasomal  
98 degradation(Komander, 2009). Several human and animal viruses encode DUB homologs that  
99 play important roles in the virus life cycle by promoting viral genome replication and inhibiting  
100 the host antiviral response(Bailey-Elkin et al., 2017; Gastaldello et al., 2010; Kattenhorn et al.,  
101 2005). In this study, we report that TOP2 interacts with and is a substrate of the DUB encoded  
102 in the N-terminal domain of the EBV large tegument protein BPLF1 and provide evidence for  
103 the capacity of BPLF1 to promote non-proteolytic pathways for the resolution of TOP2ccs,  
104 which enhances cell survival and virus replication.

105

106 **Results**

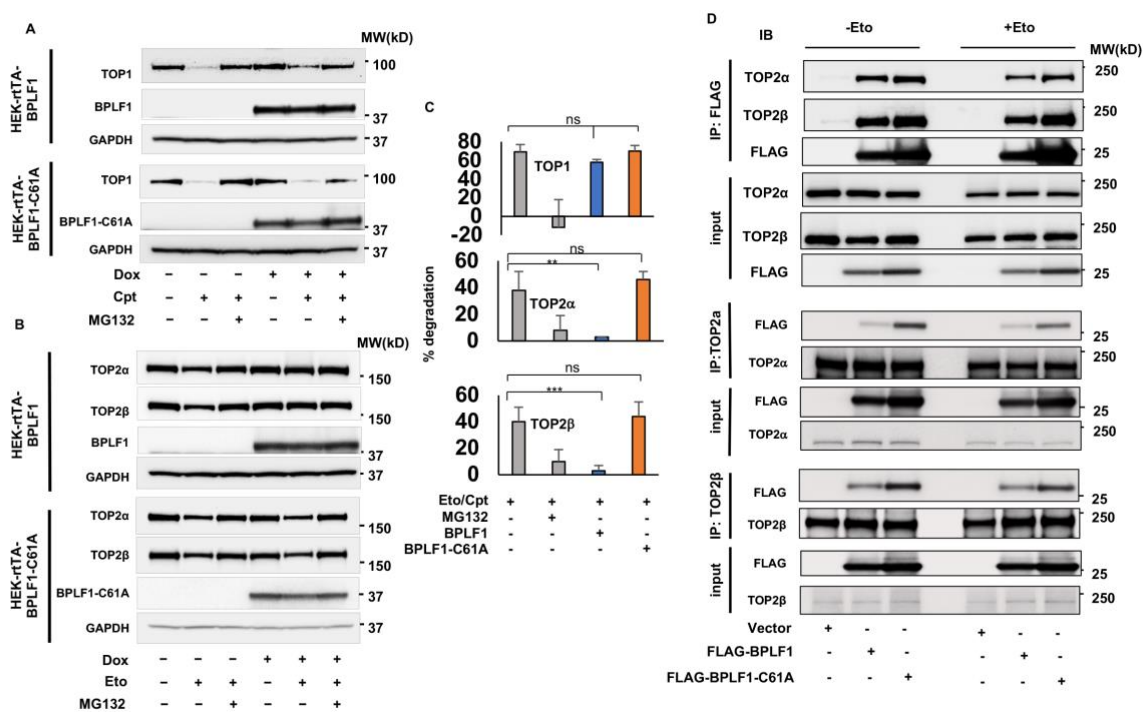
107 *BPLF1 selectively inhibits the degradation of TOP2 in cells treated with*  
108 *topoisomerase poisons*

109 To investigate whether the EBV encoded DUB regulates the proteasomal degradation of  
110 topoisomerases, FLAG-tagged versions of the 325 amino acid long N-terminal catalytic domain  
111 of BPLF1 and an inactive mutant where the catalytic Cys61 was substituted with Ala (BPLF1-  
112 C61A) were stably expressed by lentivirus transduction in HEK-293T cells under the control  
113 of a Tet-on regulated promoter (HEK-rtTA-BPLF1/BPLF1-C61A cell lines). Inducible  
114 expression was monitored by probing immunoblots of cells treated for 24 h with increasing  
115 concentration of doxycycline (Dox) with antibodies to the FLAG or V5 tags (Fig. S1A).  
116 Although the steady-state levels of BPLF1-C61A appeared to be lower, which may be due to  
117 rapid turnover, both polypeptides were readily detected by anti-FLAG immunofluorescence in  
118 approximately 50% of the induced cells, while the fluorescence was weak or below detection  
119 in the remaining cells (Fig. S1B).

120 To monitor ubiquitin-dependent proteasomal degradation, HEK-rtTA-BPLF1/BPLF1-C61A  
121 cells cultured overnight in the presence or absence of Dox were treated with the TOP1 poison  
122 Camptothecine or the TOP2 poison Etoposide in the presence or absence of the proteasome  
123 inhibitor MG132, and topoisomerase levels were assessed by western blot. Camptothecine and  
124 Etoposide trap TOP1-DNA and TOP2-DNA covalent adducts, respectively(Pommier, 2013),  
125 while MG132 prevents the proteasomal degradation of stalled topoisomerase-DNA  
126 intermediates(Mao et al., 2001). As expected, TOP1 was efficiently degraded in  
127 Camptothecine treated cells (Fig. 1A and Fig. 1C upper panels), while treatment with  
128 Etoposide promoted the degradation of both TOP2 $\alpha$  and TOP2 $\beta$  (Fig. 1B and 1C middle and

129 lower panels). The degradation was inhibited by treatment with MG132, confirming the  
 130 involvement of the proteasome in the clearance of poisoned topoisomerases. Expression of wild  
 131 type or mutant BPLF1 did not affect the Camptothecine-induced degradation of TOP1. In  
 132 contrast, expression of BPLF1 was accompanied by stabilization of both TOP2 $\alpha$  and TOP2 $\beta$  in  
 133 Etoposide-treated cells, while the mutant BPLF1-C61A had no effect. Thus, the viral DUB  
 134 selectively inhibits the degradation of TOP2 isozymes by the proteasome.

135



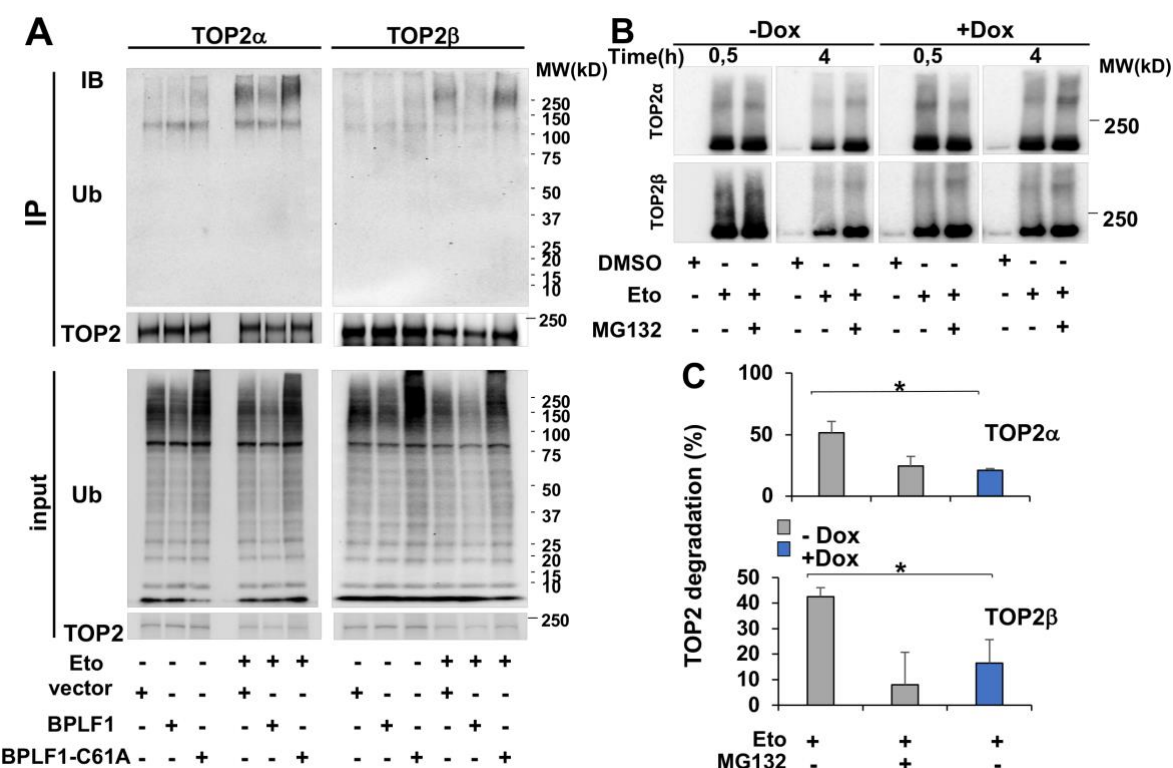
136 **Figure 1. BPLF1 selectively binds to TOP2 and inhibits the degradation of TOP2 in cells**  
 137 **treated with topoisomerase poisons.** HEK-293T cell expressing inducible FLAG-BPLF1 or  
 138 FLAG-BPLF1-C61A were seeded into 6 well plates and treated with 1.5  $\mu$ g/ml doxycycline  
 139 (Dox) for 24 h. After treatment for 3 h with 5  $\mu$ M of the TOP1 poison Camptothecine (Cpt) or  
 140 6 h with 40  $\mu$ M of the TOP2 poison Etoposide (Eto) with or without the addition of 10  $\mu$ M  
 141 MG132, protein expression was analyzed in western blots probed with the indicated antibodies.  
 142 GAPDH was used as the loading control. (A) Representative western blots illustrating the  
 143 expression of TOP1 in control and Camptothecine treated cells. The treatment induced  
 144 degradation of TOP1 by the proteasome, which was not affected by the expression of BPLF1  
 145 or BPLF1-C61A in Dox treated cells. (B) Representative western blots illustrating the

146 *expression of TOP2 $\alpha$  and TOP2 $\beta$  in Etoposide treated cells. Expression of BPLF1 reduced the*  
147 *Etoposide-induced degradation of both TOP2 $\alpha$  and TOP2 $\beta$  while BPLF1-C61A had no*  
148 *appreciable effect. (C) The percentage degradation of TOP1, TOP2 $\alpha$  and TOP2 $\beta$  in*  
149 *Camphothecine or Etoposide treated cells versus untreated controls was calculated from the*  
150 *intensity of the specific bands recorded in two (TOP1) or three (TOP2 $\alpha$  and TOP2 $\beta$ )*  
151 *independent experiments using the ImageJ software. Data from HEK-rtTA-BPLF1/BPLF1-*  
152 *C61A cultured in the absence of Dox were pulled. Statistical analysis was performed using*  
153 *Student's t-test. \*\*P< 0.01; \*\*\*P < 0.001; ns, not significant. (D) HEK293T cells transfected*  
154 *with FLAG-BPLF1, FLAG-BPLF1-C61A, or FLAG-empty vector were treated with 40  $\mu$ M*  
155 *Etoposide for 30 min and cell lysates were either immunoprecipitated with anti-FLAG*  
156 *conjugated agarose beads or incubated for 3 h with anti-TOP2 $\alpha$  or TOPO2 $\beta$  antibodies*  
157 *followed by the capture of immunocomplexes with protein-G coated beads. Catalytically active*  
158 *and inactive BPLF1 binds to both TOP2 $\alpha$  and TOP2 $\beta$  in both untreated and Etoposide treated*  
159 *cells (upper panels). Conversely, TOP2 $\alpha$  (middle panels) and TOP2 $\beta$  (lower panels) interacts*  
160 *with both catalytically active and inactive BPLF1. Representative western blots from one of*  
161 *two independent experiments where all conditions were tested in parallel are shown.*

162 ***TOP2 is a BPLF1 substrate***

163 To assess whether topoisomerases are direct substrates of BPLF1, we first investigated whether  
164 they interact in cells and in pull-down assays performed with recombinant proteins. Lysates of  
165 HEK-293T cells transiently transfected with FLAG-BPLF1 or FLAG-BPLF-C61A were  
166 immunoprecipitated with antibodies recognizing FLAG, TOP1, TOP2 $\alpha$  or TOP2 $\beta$ . In line with  
167 the failure to rescue Camphothecine-induced degradation, BPLF1 did not interact with TOP1  
168 (Fig. S2A), whereas both TOP2 $\alpha$  and TOP2 $\beta$  were readily detected in western blots of the  
169 FLAG immunoprecipitates and, conversely, BPLF1 was strongly enriched in the TOP2 $\alpha$  and  
170 TOP2 $\beta$  immunoprecipitates indicating that the proteins interact in cells (Fig. 1D). Of note, co-  
171 immunoprecipitation was more efficient when BPLF1-C61A was the bait, suggesting that  
172 TOP2 may be a substrate of the viral enzyme. To gain insight on the nature of the interaction,  
173 equimolar concentration of yeast expressed FLAG-TOP2 $\alpha$ , or a TOP2 $\alpha$  mutant lacking the

174 unique C-terminal domain that is not conserved in the TOP2 $\beta$  isozyme, FLAG-TOP2 $\alpha$ - $\Delta$ CTD,  
175 were mixed with bacterially expressed His-BPLF1 and reciprocal pull-downs were performed  
176 with anti-FLAG (Fig. S2B) or Ni-NTA coated beads (Fig. S2C). A weak BPLF1 band was  
177 reproducibly detected in western blots of the FLAG-TOP2 $\alpha$  pull-downs probed with a His-  
178 specific antibody and, conversely, a weak FLAG-TOP2 $\alpha$  band was detected in the His pull-  
179 downs. The binding of BPLF1 to TOP2 $\alpha$  was not affected by deletion of the TOP2 $\alpha$  C-terminal  
180 domain (Fig. S2D), pointing to a TOP2 $\alpha$  and TOP2 $\beta$  shared domain shared as the likely site of  
181 interaction. Notably, comparison of the efficiency of *in vitro* pull-down versus co-  
182 immunoprecipitation suggests that binding may be stabilized by factors or TOP2 modifications  
183 that are only present in cell lysates. To further investigate whether the viral DUB  
184 deubiquitinates TOP2, BPLF1, TOP2 $\alpha$  and TOP2 $\beta$  were immunoprecipitated from lysates of  
185 control and Etoposide-treated HEK-293T cells transiently transfected with BPLF1 or BPLF1-  
186 C61A and western blots were probed with a ubiquitin-specific antibody. The cell lysates were  
187 prepared under denaturing conditions to exclude non-covalent protein interactions and working  
188 concentrations of NEM and iodoacetamide were added to all buffers to inhibit DUB activity.  
189 In line with the capacity of Etoposide to promote the proteasomal degradation of TOP2, smears  
190 of high molecular weight species corresponding to ubiquitinated TOP2 $\alpha$  and TOP2 $\beta$  were  
191 detected in the immunoprecipitates of Etoposide-treated cells (Fig. 2A). The intensity of the  
192 smears was strongly decreased in cells expressing catalytically active BPLF1, while the mutant  
193 BPLF1-C61A had no appreciable effect, confirming that TOP2 is a bona-fide BPLF1 substrate.



194 **Figure 2. BPLF1 deubiquitinates TOP2 and stabilizes TOP2cc.** (A) HEK293T cells were  
195 transiently transfected with plasmids expressing FLAG-BPLF1, FLAG-BPLF1-C61A, or the  
196 empty FLAG vector, and aliquots were treated with 40  $\mu$ M Etoposide for 30 min. TOP2 $\alpha$  and  
197 TOP2 $\beta$  were immunoprecipitated from cell lysates prepared under denaturing conditions in the  
198 presence of DUB inhibitors and western blots were probed with antibodies to TOP2 $\alpha$ , TOP2 $\beta$   
199 and ubiquitin. The expression of catalytically active BPLF1 inhibits the ubiquitination of  
200 TOP2 $\alpha$  and TOP2 $\beta$  in Etoposide treated cells. Western blots from one representative  
201 experiment out of three are shown in the figure. (B) HEK-rtTA-BPLF1 cells were treated with  
202 1.5  $\mu$ g/ml Dox for 24 h followed by treatment with 80  $\mu$ M Etoposide for the indicated time with  
203 or without the addition of 10  $\mu$ M MG132. RADAR assays were performed as described in  
204 Materials and Methods and TOP2 trapped in 10  $\mu$ g DNA was detected in western blots using  
205 antibodies to TOP2 $\alpha$  or TOP2 $\beta$ . Trapped TOP2 appeared as a major band of the expected size  
206 and a smear of higher molecular weight species. The intensity of the trapped TOP2 $\alpha$  and  
207 TOP2 $\beta$  bands decrease over time in control untreated cells due to proteasomal degradation,  
208 while the decrease was significantly reduced upon expression of BPLF1 in Dox treated cells.  
209 Western blots from one representative experiment out of two are shown in the figure. (C) The  
210 percentage of Etoposide-induced TOP2 degradation was calculated from the intensity of the  
211 specific bands measured with the ImageJ software. MG132 prevented the degradation of

212 *TOP2 $\alpha$  and TOP2 $\beta$  trapped into TOP2cc in control BPLF1 negative cells whereas TOP2*  
213 *degradation was significantly reduced in BPLF1 expressing cells. The mean $\pm$ SD of two*  
214 *independent experiments is shown in the figure.*

215

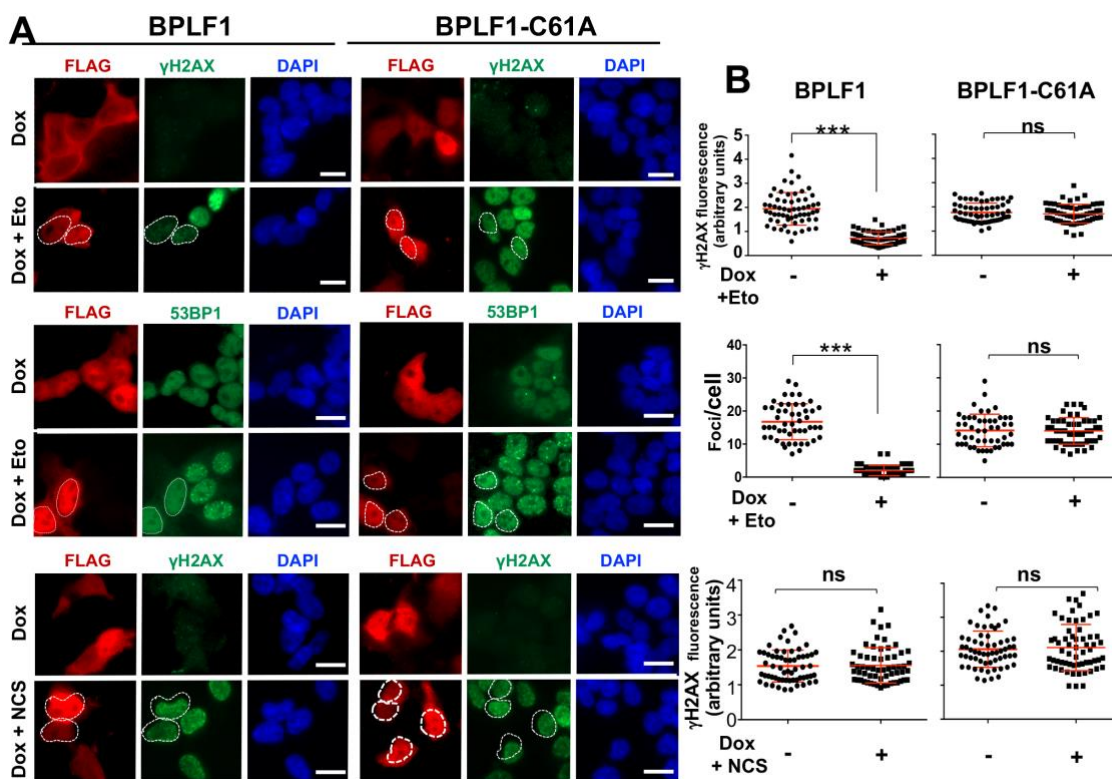
216 Degradation of TOP2 by the proteasome plays an important role in the debulking of persistent  
217 TOP2ccs generated by topoisomerase poisons. To investigate whether the viral DUB may  
218 interfere with this process, HEK-rtTA-BPLF1 cells cultured for 24 h in the presence or absence  
219 of Dox were treated for 30 min or 4 h with Etoposide with or without addition of MG132, and  
220 DNA-trapped TOP2 was detected by RADAR (rapid approach to DNA adduct recovery)  
221 assays(Anand et al., 2018). Neither TOP2 $\alpha$  nor TOP2 $\beta$  were detected in control DMSO treated  
222 cells confirming that only covalently DNA-bound species are isolated by this method (Fig. 2B).  
223 In Etoposide treated cells, TOP2 $\alpha$  and TOP2 $\beta$  appeared as major bands of the expected size  
224 and smears of high molecular weight species that are likely to correspond to different types of  
225 post-translational modifications. Comparable amounts of trapped TOP2 $\alpha$  and TOP2 $\beta$  were  
226 detected in cells treated with Etoposide for 30 min, independently of BPLF1 expression or  
227 MG132 treatment, indicating that neither treatment, either alone or in combination, affects the  
228 formation of TOP2ccs. As expected, the intensity of the TOP2 band decreased after Etoposide  
229 treatment for 4 h, which was inhibited by MG132, confirming the involvement of proteasome-  
230 dependent degradation in the debulking of Etoposide-induced TOP2ccs. The degradation of  
231 both TOP2 $\alpha$  and TOP2 $\beta$  was significantly decreased at the 4 h time point in Dox treated cells,  
232 resulting in levels of stabilization comparable to those achieved by treatment with MG132 (Fig.  
233 2C). Thus, BPLF1 deubiquitinates and stabilizes TOP2 trapped in covalent DNA adducts. The  
234 finding was independently confirmed in experiments where TOP2ccs were stabilized by  
235 alkaline lysis(Ban et al., 2013) (Fig. S3A). Smears of high molecular weight species were  
236 readily detected above the main TOP2 $\beta$  band in Dox-induced Etoposide-treated HEK-rtTA-

237 BPLF1 cells, whereas high molecular weight species were not detected when the blots were  
238 probed with a TOP1 specific antibody, confirming that the high molecular weight species  
239 correspond to DNA-trapped TOP2 (Fig. S3A). As expected, the intensity of the high molecular  
240 weight species decreased with time in BPLF1 negative cells, and the decrease was inhibited by  
241 MG132 confirming the involvement of proteasomal degradation. In cells expressing  
242 catalytically active BPLF1, the intensity of the high molecular weight species remained  
243 virtually constant over the observation time, resulting in significantly higher amounts of  
244 residual TOP2ccs (Fig. S3B). Similar results were obtained when the blots were probed with  
245 antibodies to TOP2 $\alpha$ .

246 *BPLF1 inhibits the detection of Etoposide-induced DNA damage and promotes*  
247 *TOP2 SUMOylation and cell survival*

248 The removal of TOP2 trapped in TOP2ccs induces a DNA damage response (DDR) that, while  
249 limiting Etoposide toxicity, may also promote genomic instability and apoptosis(Lee et al.,  
250 2016; Mao et al., 2001; Sciascia et al., 2020). To test whether the capacity of BPLF1 to stabilize  
251 TOP2ccs interferes with DDR activation, HEK-rtTA-BPLF1/BPLF-C61A cells cultured in the  
252 presence or absence of Dox for 24 h and then treatment with Etoposide for 1 h. The  
253 accumulation of phosphorylated histone H2AX ( $\gamma$ H2AX), a validated DDR marker(Mah et al.,  
254 2010), was monitored by immunofluorescence in BPLF1 positive and negative cells. As  
255 illustrated by representative fluorescence micrographs (Fig. 3A, upper panels) and plots of  
256 fluorescence intensity in BPLF1 positive and negative cells (Fig. 3B, upper panels), a diffuse

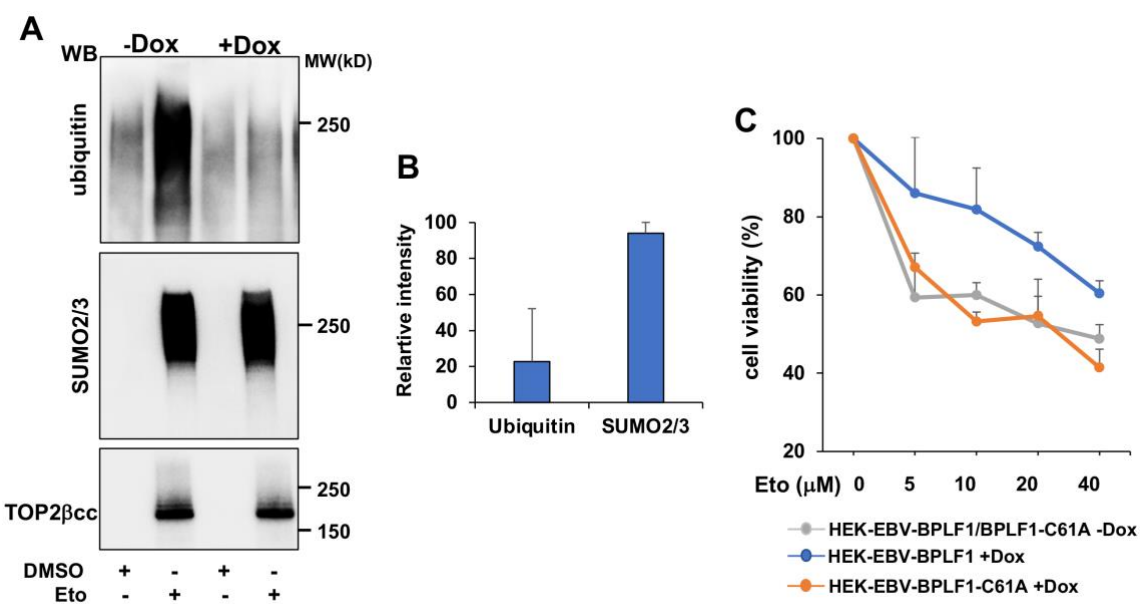
257  $\gamma$ H2AX fluorescence was readily detected in Etoposide-treated BPLF1 negative cells and in  
258 cells expressing the mutant BPLF-C61A.



259 **Figure 3. BPLF1 selectively inhibits the detection of TOP2-induced DNA damage.** HEK-  
260 *rtTA-BPLF1/BPLF1-C61A* cells grown on cover-slides were treated with 1.5  $\mu$ g/ml Dox for 24  
261 h to induce the expression of BPLF1 followed by treatment for 1 h with 40  $\mu$ M Etoposide or  
262 0.5  $\mu$ g/ml of the radiomimetic Neocarzinostatin (NCS) before staining with the indicated  
263 antibodies. (A) The cells were co-stained with antibodies against FLAG (red) and antibodies  
264 to  $\gamma$ H2AX or 53BP1 (green) and the nuclei were stained with DAPI (blue). Expression of the  
265 catalytically active BPLF1 was associated with a significant decrease of nuclear  $\gamma$ H2AX  
266 fluorescence and decreased formation of 53BP1 foci while the BPLF1-C61A mutant had no  
267 effect. Neither the catalytically active nor the inactive BPLF1 affected the induction of  $\gamma$ H2AX  
268 in cells treated with NCS. Representative micrographs from one out of two experiments where  
269 all conditions were tested in parallel are shown. Scale bar = 10  $\mu$ m. (B) Quantification of  
270  $\gamma$ H2AX fluorescence intensity and 53BP1 foci in BPLF1/BPLF1-C61A positive and negative  
271 cells from the same image. The Mean  $\pm$  SD of fluorescence intensity in at least 50 BPLF1-  
272 positive and 50 BPLF1-negative cells recorded in each condition is shown. Statistical analysis  
273 was performed using Student's t-test. \*\*\*P < 0.001; ns, not significant.

274 Cells expressing active BPLF1 showed significantly weaker  $\gamma$ H2AX fluorescence, suggesting  
275 that the viral enzyme counteracts DDR activation. Accordingly, DNA repair was not triggered  
276 as assessed by the impaired formation of 53BP1 foci in BPLF1 positive compared to negative  
277 cells (Fig. 3A and 3B, middle panels). A comparable BPLF1-dependent decrease of  $\gamma$ H2AX  
278 fluorescence and formation of 53BP1 and BRCA1 foci was observed upon Etoposide treatment  
279 in HeLa cells transiently transfected with BPLF1/BPLF1-C61A (Fig. S4), confirming that the  
280 effect is not cell-type specific. To assess whether the failure to activate the DDR may be due to  
281 the capacity of BPLF1 to target events downstream of the formation of DSBs, cells expressing  
282 BPLF1/BPLF1-C61A were treated with the radiomimetic agent Neocarzinostain (NCS)(Povirk,  
283 1996). Neither BPLF1 nor BPLF1-C61A altered the induction of  $\gamma$ H2AX in NCS treated cells  
284 (Fig. 3A and 3B, lower panels). Thus, BPLF1 selectively inhibits the DDR and DNA repair  
285 responses triggered by Etoposide-induced DSBs.

286 In the absence of TOP2 degradation, TOP2cc may be resolved via a non-proteolytic process  
287 whereby SUMOylation-dependent conformational changes expose the tyrosyl-DNA bond to  
288 the activity of Tyrosyl-DNA-phosphodiesterase-2 (TDP2), which enables DSBs repair without  
289 the need of nuclease activity(Schellenberg et al., 2017). To assess whether this pathway may  
290 be engaged in BPLF1 expressing cells, Dox-treated HEK-rtTA-BPLF1 cells were exposed to  
291 Etoposide for 30 min and western blots of TOP2ccs isolated by RADAR were probed with  
292 antibodies to ubiquitin and SUMO2/3. As expected, smears of high molecular weight species  
293 reacting with both ubiquitin- and SUMO2/3-specific antibodies were highly enriched in  
294 Etoposide treated cells (Fig. 4A).



295 **Figure 4. BPLF1 promotes TOP2 SUMOylation and cell viability following Etoposide**  
296 **treatment.** (A) HEK-rtTA-BPLF1 cells were cultured for 24 h in the presence or absence of 1.5  
297  $\mu\text{g/ml}$  Dox and then treated with 80  $\mu\text{M}$  Etoposide for 30 min followed by detection of DNA  
298 trapped TOP2 by RADAR assay. Western blots of proteins bound to 10  $\mu\text{g}$  DNA were probed  
299 with antibodies to ubiquitin, SUMO2/3 and TOP2. The expression of BPLF1 was associated  
300 with strongly decreased ubiquitination of the TOP2ccs while SUMOylation was only  
301 marginally affected. (B) The intensity of the ubiquitin, SUMO2/3 and TOP2bcc specific bands  
302 was quantified by densitometry using the ImageJ software. Relative intensity was calculated as  
303 the % intensity in Dox-treated versus untreated cells after normalization to TOP2cc. Mean  $\pm$   
304 SD of two independent experiments. (C) HEK-rtTA-BPLF1/BPLF1-C61A cells were cultured  
305 for 24 h in the presence or absence of 1.5  $\mu\text{g/ml}$  Dox and then treated overnight with the  
306 indicated concentration of Etoposide before assessing cell viability by MTT assays. The  
307 expression of catalytically active BPLF1 decreased the toxic effect of Etoposide over a wide  
308 range of concentrations while BPLF1-C61A had no appreciable effect. The mean  $\pm$  SD of two  
309 independent experiments is shown.

310

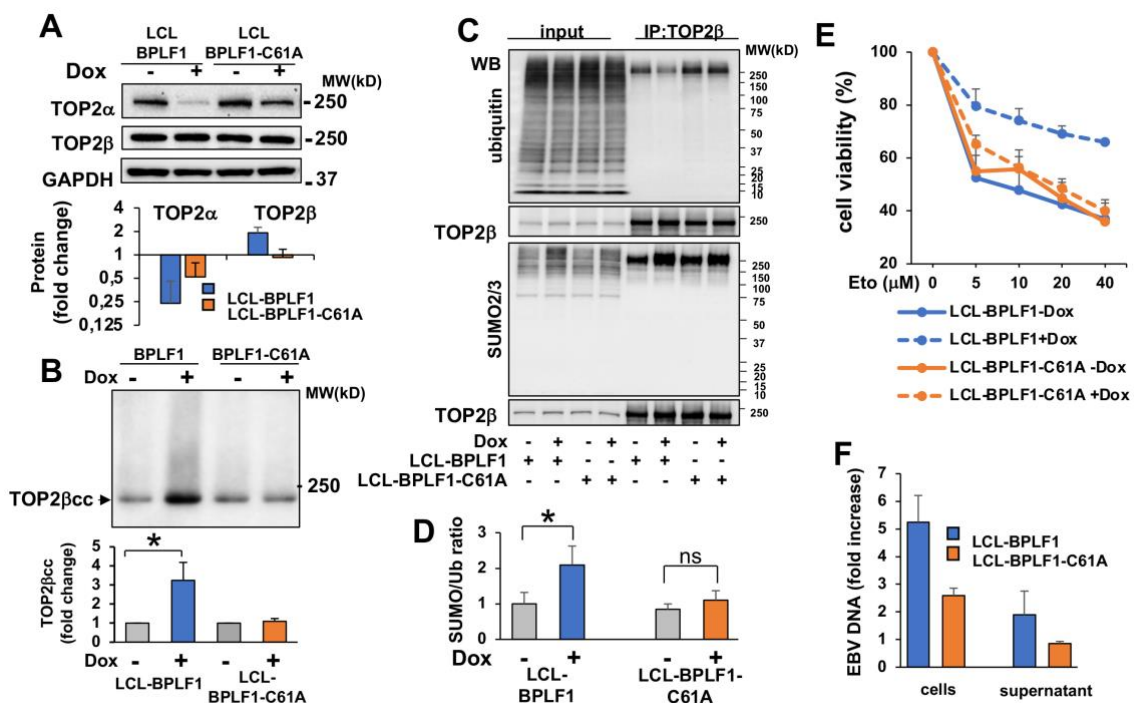
311 Although the formation of TOP2ccs was not affected (Fig. 4A, lower panel), expression of the  
312 viral DUB was accompanied by a dramatic decrease of ubiquitinated species, while the intensity  
313 of the SUMO2/3 smear was largely unaffected (Fig 4A upper and middle panels and 4B). Thus,  
314 in addition to preventing the detection of TOP2-induced DNA damage, by inhibiting TOP2

315 ubiquitination BPLF1 may shift the processing of TOP2ccs towards non-proteolytic pathways,  
316 which could counteract the toxic effect of Etoposide. To test this possibility, cell viability was  
317 assessed by Thiazolyl blue tetrazolium bromide (MTT) assays in untreated and Dox-induced  
318 HEK-rtTA-BPLF1/BPLF1-C61A cells following overnight exposure to increasing  
319 concentrations of Etoposide. Similar levels of cell viability were observed in cells treated with  
320 Etoposide in the absence of Dox whereas, in line with the hypothesized protective effect of  
321 BPLF1, cell viability was consistently improved in cells expressing the active enzyme over a  
322 wide range of Etoposide concentrations and the BPLF1-C61A mutant had no appreciable effect  
323 (Fig. 4C).

324 *BPLF1 regulates the activity of TOP2 $\beta$  during productive infection*

325 In the final set of experiments, we asked whether physiological levels of BPLF1 regulate the  
326 activity of TOP2 during the productive virus cycle in EBV infected cells. To this end, infectious  
327 virus rescued from HEK-293-EBV cells carrying recombinant EBV expressing wild type or  
328 mutant BPLF1(Gupta et al., 2018) was used to transform normal B-lymphocytes into  
329 immortalized lymphoblastoid cell lines (LCL-EBV-BPLF1/BPLF1-C61A). To optimize the  
330 induction of the productive virus cycle, the LCLs were stably transduced with a recombinant  
331 lentivirus expressing the viral transactivator BZLF1 under the control of a tetracycline-  
332 regulated promoter. Treatment with Dox induced the expression of early (BMRF1) and late  
333 (BFRF3) viral antigens detected in western blots probed with specific antibodies (Fig. S5A),  
334 and BPLF1 mRNA detected by qPCR (Fig. S5B). Of note, the induction of late antigens was  
335 consistently weaker in LCL-EBV-BPLF1-C61A (Fig. S5A), pointing to impairment of the late  
336 phase of the virus cycle.

337 Consistent with the establishment of a pseudo-S-phase where progression to G2/M is blocked  
 338 and cellular DNA synthesis is inhibited(Kudoh et al., 2003), induction of the productive cycle  
 339 was associated with a strong decrease of TOP2 $\alpha$  mRNA (Fig. S5C) and protein levels (Fig. 5A)  
 340 while TOP2 $\beta$  protein and mRNA showed either no change or a small increase of protein levels  
 341 in cells expressing catalytically active BPLF1 (Fig. 5A and S5C).



342

343 **Figure 5. BPLF1 regulates the expression and activity of TOP2 $\beta$  during productive infection.**  
 344 The productive virus cycle was induced by treatment with 1.5 mg/ml Dox in LCL cells carrying  
 345 recombinant EBV encoding wild type or catalytic mutant BPLF1 and expressing a tetracycline  
 346 regulated BZLF1 transactivator. (A) The expression of TOP2 $\alpha$  and TOP2 $\beta$  was assessed by  
 347 western blot and the intensity of the specific bands was quantified using the ImageJ software.  
 348 Induction of the productive cycle was associated with a highly reproducible downregulation of  
 349 TOP2 $\alpha$  while TOP2 $\beta$  was either unchanged or slightly increased. The effect was stronger in  
 350 cells expressing wild type BPLF1. Representative western blots and quantification of specific  
 351 bands in three to five independent experiments are shown. (B) The formation of TOP2bcc was  
 352 investigated by RADAR assays in untreated and induced LCLs. Representative western blot  
 353 illustrating the significant increase of TOP2bcc upon induction of the productive virus cycle in

354 *LCL cells expressing catalytically active BPLF1. BPLF1-C61A had no appreciable effect. One*  
355 *representative western blots and quantification of the intensity of the TOP2b smears in three*  
356 *independent experiments are shown. Fold increase was calculated as the ratio between the*  
357 *smear intensity in control versus induced cells. \*P<0.05. (C) TOP2 $\beta$  was immunoprecipitated*  
358 *from total cell lysates of control and induced LCLs and western blots were probed with*  
359 *antibodies to TOP2 $\beta$ , ubiquitin and SUMO2/3. Western blots illustrating the decreased*  
360 *ubiquitination and increased SUMOylation of TOP2 $\beta$  in cells expressing catalytically active*  
361 *BPLF1. One representative experiment out of three is shown. (D) The intensity of the bands*  
362 *corresponding to immunoprecipitated TOP2 $\beta$ , ubiquitinated and SUMOylated species was*  
363 *quantified using the ImageJ software and the SUMO/Ub ratio was calculated after*  
364 *normalization to the intensity of immunoprecipitated TOP2b. The mean  $\pm$  SD of three*  
365 *independent experiments is shown. \*P<0.05. (E) The productive cycle was induced in LCL-*  
366 *EBV-BPLF1/BPLF1-C61A by culture for 72 h in the presence 1.5  $\mu$ g/ml Dox. After washing*  
367 *and counting, 5x10<sup>4</sup> live cells were seeded in triplicate wells of 96 well plates and treated*  
368 *overnight with the indicated concentration Etoposide before assessing cell viability by MTT*  
369 *assays. The expression of catalytically active BPLF1 enhanced cell viability over a wide range*  
370 *of Etoposide concentration with BPLF1-C61A had no appreciable effect. The mean  $\pm$  SD of*  
371 *cell viability in three independent experiments is shown. (F) The amount of cell associated and*  
372 *release EBV DNA was measures in the cell pellets ad supernatants after induction for 72 h.*  
373 *Fold induction was calculated relative to uninduced cells. Mean  $\pm$  DS of 3 experiments.*

374

375 This was associated with a significant increase of TOP2 $\beta$ ccs relative to uninduced cells or cells  
376 expressing the mutant BPLF1-C61A (Fig. 5B), and with decreased TOP2 $\beta$  ubiquitination (Fig.  
377 5C top panel). As previously reported, higher molecular weight species detected by the  
378 SUMO2/3 specific antibody were increased in induced cells due to viral micro-RNA-dependent  
379 downregulation of RNF4(Li et al., 2017). SUMOylated species were also increased in  
380 immunoprecipitated TOP2 $\beta$  (Fig. 5C lower panel), resulting in a significant shift of the  
381 SUMO/ubiquitin ratio towards TOP2 $\beta$  SUMOylation in cells expressing catalytically active  
382 BPLF1 (Fig. 5D). As observed with the inducible HEK-rtTA-BPLF1 cell line, expression of

383 the active viral DUB counteracted the toxic effect of Etoposide (Fig. 5E). Furthermore, the  
384 BPLF1-mediated regulation of TOP2 $\beta$  expression and ubiquitination was associated with  
385 higher levels of viral DNA replication and efficient release of infectious virus particles as  
386 measured by qPCR in cell pellets and culture supernatants (Fig. 5F).

387

## 388 **Discussion**

389 Although compelling evidence points to a pivotal role of topoisomerases in the replication of  
390 herpesviruses and other DNA viruses(M. Kawanishi, 1993; Wang et al., 2009; Wang et al.,  
391 2008), very little is known about the mechanisms by which the viruses harness the activity of  
392 these cellular enzymes. In this study, we have shown that the ubiquitin deconjugases encoded  
393 in the N-terminal domain of the EBV large tegument protein BPLF1 regulates the activity of  
394 TOP2 $\beta$  during productive EBV infection by promoting the proteasome-independent debulking  
395 of TOP2-DNA adducts, which favors cell survival and the faithful replication and transcription  
396 of viral DNA. The findings highlight a previously unrecognized function of the viral enzyme  
397 in hijacking cellular functions that enable efficient virus production. Our proposed model for  
398 the activity of BPLF1 is shown in Fig. 6.

399

400 We found that the viral DUB that is physiologically released during productive infection via  
401 caspase-1-mediated cleavage of the EBV large tegument protein BPLF1(Gastaldello et al.,  
402 2013) selectively binds to TOP2 $\alpha$  and TOP2 $\beta$ , and effectively counteracts their ubiquitination  
403 and proteasomal degradation in cells treated with Etoposide (Fig. 1, Fig 2A). In the absence of  
404 proteasomal degradation, TOP2ccs were stabilized (Fig 2B, 2C), which prevented the  
405 unmasking of TOP2-induced DSBs (Fig 3) and promoted resistance to the toxic effect of

406 Etoposide (Fig 4C). Several lines of evidence suggest that the potent DDR triggered by the  
407 proteolytic debulking of TOP2ccs may be detrimental to cell survival and genomic integrity.  
408 Following the degradation of TOP2, protein-free DSBs engage multiple pathways for error-free  
409 or error-prone repair, including MRE11 nuclease-dependent homologous recombination  
410 (HR)(Hoa et al., 2016) and non-homologous end joining (NHRJ)(Gomez-Herreros et al., 2013;  
411 Gomez-Herreros et al., 2017). Recent findings suggest that a substantial fraction of the  
412 Etoposide induced DSBs undergo extensive DNA end-resection(Sciascia et al., 2020), which  
413 favors mispairing and the occurrence of chromosomal rearrangements that compromise cell  
414 viability or promote genomic instability. Of note, these genotoxic effects were efficiently  
415 counteracted by inhibition of the proteasome prior or during Etoposide treatment, supporting  
416 the notion that the non-proteolytic resolution of TOP2ccs can minimize DSB misrepair and  
417 promote genomic integrity(Sciascia et al., 2020).

418

419 We found that expression of the catalytically active viral deubiquitinase closely mimicked the  
420 stabilization of TOP2ccs (Fig 2B) and inhibition of both DDR activation (Fig. 3) and Etoposide  
421 toxicity (Fig. 4C and 5E) observed upon inhibition of the proteasome. While in line with the  
422 notion that ubiquitination is strictly required for the targeting of substrates to the proteasome,  
423 this finding points to the capacity of BPLF1 to shift the cellular strategy for TOP2cc debulking  
424 towards proteasome-independent pathways that may ensure higher fidelity of DNA repair and  
425 reduce toxicity. In this context, it is important to notice that, while inhibiting ubiquitination,  
426 catalytic active BPLF1 did not affect the SUMOylation of TOP2cc in Etoposide treated cells  
427 (Fig. 4A) and promoted the preferential SUMOylation of TOP2 $\beta$  during productive EBV  
428 infection (Fig. 5C and 5D). SUMOylation plays multiple roles in the debulking of TOP2ccs. It  
429 may mediate TOP2 proteolysis by serving as a recognition signal for ubiquitination mediated  
430 by SUMO-targeted ubiquitin ligases such as RNF4(Sun, Miller Jenkins, et al., 2020) or may

431 recruit SprT-family metalloproteases, such as SPRTN(Lopez-Mosqueda et al., 2016) and  
432 ARC/GCNA(Borgermann et al., 2019), that are involved in the proteasome-independent  
433 proteolytic debulking of DNA-protein adducts. Interestingly, the activity of SPRTN is inhibited  
434 by mono-ubiquitination(Stingele et al., 2016) and yet unpublished findings suggest that failure  
435 to deubiquitinate SPRTN upon depletion of the cellular deubiquitinase USP11 leads to the  
436 accumulation of unrepaired DNA-protein adducts(Perry et al., 2020). Thus, BPLF1 could  
437 mimic the activity of the cellular DUB. In addition, SUMOylation of TOP2 by the ZNF451  
438 ligase was shown to promote the non-proteolytic resolution of TOP2-DNA cross-links via  
439 direct recruitment of TDP2 through a “split-SIM” SUMO2 engagement platform(Schellenberg  
440 et al., 2017). SUMOylation was shown to alter the conformation of the trapped TOP2 dimers,  
441 thereby facilitating the access of TDP2 to the tyrosyl-DNA covalent bond and promoting error-  
442 free rejoicing of the DSBs. This may be accomplished by the T4 DNA ligase(Gomez-Herreros  
443 et al., 2013) or, upon removal of Etoposide, by TOP2 (Sciascia et al., 2020).

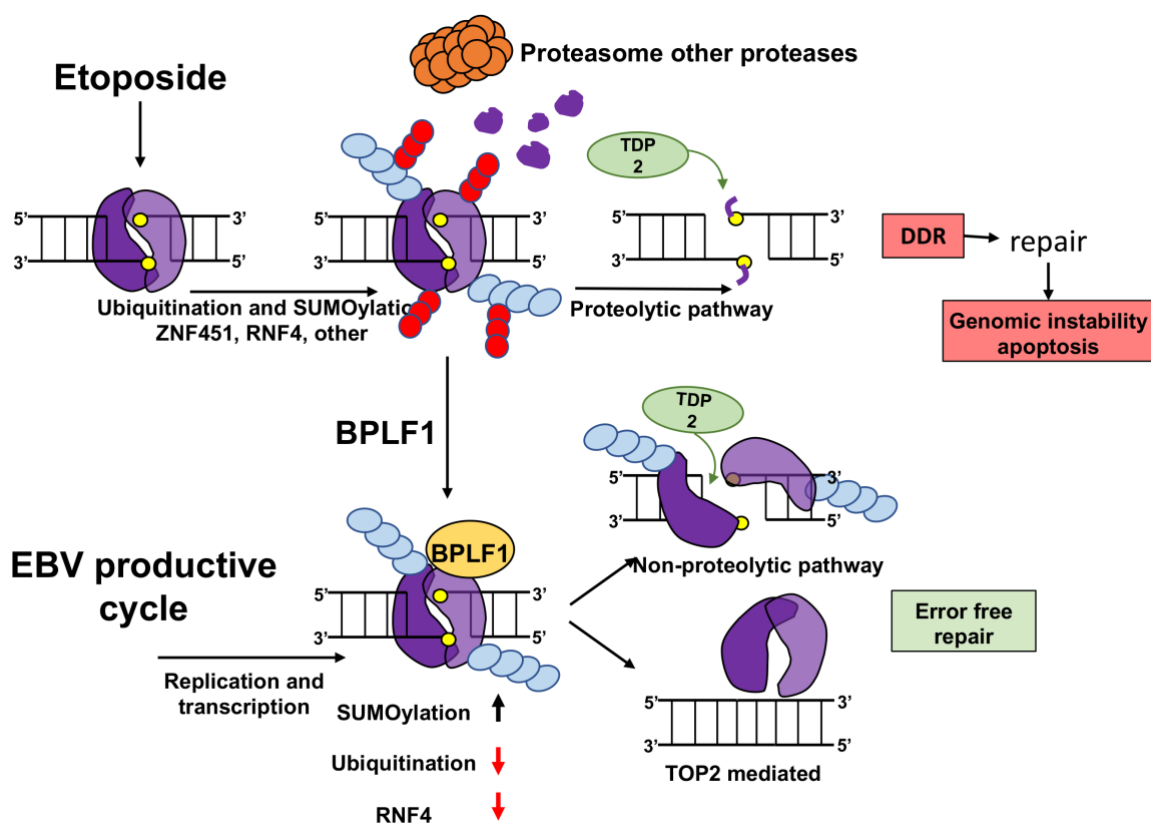
444

445 While the pivotal role of topoisomerases in both the latent and lytic replication of herpesviruses  
446 is firmly established(Benson & Huang, 1988; Ebert et al., 1990; M Kawanishi, 1993), the roles  
447 of the individual enzymes are not well understood. The torsion-relieving activity of TOP1 was  
448 shown to be essential for reconstitution of the HSV replication machinery using purified viral  
449 proteins(Nimonkar & Boehmer, 2004), and its recruitment to the viral replication complex was  
450 required for the lytic origin (OriLyt)-driven replication of EBV(Wang et al., 2009) and  
451 KSHV(Wang et al., 2008). Less is known about the function of the TOP2 isozymes, although  
452 the importance of TOP2 is underscored by its upregulation during the productive cycle of  
453 HCMV(Benson & Huang, 1990) and KSHV(Wang et al., 2008) despite a general host proteins  
454 shutoff during virus replication. We have found that TOP2 $\alpha$  mRNA is strongly downregulated  
455 upon induction of the productive virus cycle in EBV infected cells (Fig. S5C) and the protein

456 becomes virtually undetectable in cells expressing catalytically active BPLF1 (Fig. 5A). While  
457 possibly related to the virus-induced arrest of the cell cycle in G1/S, the precise mechanism of  
458 this downregulation remains unknown. Nevertheless, our findings exclude a major role of  
459 TOP2 $\alpha$  in the replication of the viral genome. In contrast, the expression of TOP2 $\beta$  was either  
460 not affected or slightly upregulated during productive infection, which is in line with the  
461 exclusive expression of this topoisomerase in resting cells and its essential role in transcription.  
462 Most importantly, we found that catalytically active BPLF1 was required for the accumulation  
463 of TOP2 $\beta$ ccs in cell entering the productive cycle (Fig 5B), which, in the absence of  
464 topoisomerase poisons, is likely to indicate a significant increase of TOP2 $\beta$  activity driven by  
465 viral DNA replication and/or transcription. Conceivably, the capacity of BPLF1 to stabilize  
466 TOP2ccs and their resolution by non-proteolytic pathways that favor error-free repair and cell  
467 survival may be instrumental to ensure faithful and proficient replication and transcription of  
468 the viral genome. Of note, the BPLF1-mediated salvage of TOP2 $\beta$  from proteolytic disruption  
469 is likely to be reinforced by the concomitant downregulation of RNF4(Li et al., 2017), which  
470 may ensure that sufficient levels of the protein remain available throughout the productive cycle  
471 to sustain efficient virus production.

472

473 Aberrant expression of BPLF1 in the context of abortive lytic cycle reactivation has been  
474 reported in EBV associated malignancies such as undifferentiated nasopharyngeal carcinoma,  
475 NK-T cell lymphomas, and a subset of gastric cancers<sup>(Peng et al., 2019),(Borozan et al., 2018)</sup>. Etoposide  
476 and other topoisomerase poisons are used clinically as therapeutic anticancer agents against  
477 these malignancies(Delgado et al., 2018). Our data suggest that the expression of BPLF1 could  
478 be potentially used as a biomarker to predict the effectiveness of chemotherapeutic regimens  
479 that incorporate topoisomerase poison.



480 **Figure 6. Model of TOP2 regulation by the BPLF1.** TOP2 (violet) trapped in TOP2ccs  
481 (yellow) is targeted for proteasomal degradation via SUMOylation (light blue) and  
482 ubiquitination (red) mediated by the SUMO ligase ZNF451, the SUMO-targeting ubiquitin  
483 ligase RNF4 and other cellular ubiquitin ligases, leading to the display of partially digested 5'-  
484 phosphotyrosyl-DNA adducts. Processing by the TDP2 resolvase generates protein-free DSBs  
485 that trigger the DDR and error-free or error-prone DNA repair. Imprecise repair leads to  
486 apoptosis and genomic instability. BPLF1 inhibits the degradation of Etoposide-poisoned  
487 TOP2, which inhibits activation of the DDR. In the absence of proteasomal degradation,  
488 SUMOylation may alter the conformation of the TOP2 dimer allowing direct access of TDP2  
489 to the 5'-phosphotyrosyl-DNA bonds, which promotes error-free repair. During productive  
490 EBV infection, the concomitant expression of BPLF1 and downregulation of RNF4 favors the  
491 accumulation of SUMOylated TOP2 $\beta$  and the activation of non-proteolytic pathways for  
492 TOP2ccs debulking, which, in the absence of TOP2 poisons, may be mediated by TOP2 itself.  
493 This ensures the fidelity of virus replication and transcription and enhances cell survival and  
494 virus production.

495

496 **Acknowledgements**

497 We are deeply grateful to Dr Arne Lindquist and Prof Nico Dantuma (CMB, Karolinska  
498 Institutet) for generously sharing knowledge and reagents and to Ms. Lisa Wohlgemuth (Ulm  
499 University, Germany) for technical assistance. This investigation was supported by grants  
500 awarded by the Swedish Cancer Society and The Medical Research Council. The work of SG  
501 and TH was partially supported by a grant awarded to the European ERA-NET eDEVILLI  
502 consortium.

503

504  
505 **Materials and Methods**  
506

507 *Chemicals*

508 IGEPAL CA-630 (NP40, I3021), Sodium dodecyl sulphate (SDS, L3771), N-Ethylmaleimide  
509 (NEM, E1271), Iodoacetamide (I1149), Sodium deoxycholate monohydrate ( D5670), Triton  
510 X-100 (T9284), Bovine serum albumin (BSA, A7906), Tween-20 (P9416), Trizma base (Tris,  
511 93349), Ethylenediaminetetraacetic acid disodium salt dehydrate (EDTA-E4884), Doxycycline  
512 cyclate (D9891), MG132 (M7449), Etoposide (E1383), Neocarzinostain (N9162) and  
513 Imidazole (I5513), were purchased from Sigma-Aldrich (St. Louis, MO, USA). RNase A  
514 (12091-021) and DNazol (10503027) were purchased from Invitrogen (Carlsbad, CA, USA).  
515 Micrococcal nuclease (88216) was from Thermo Fisher Scientific (Rockford, IL, USA).  
516 Complete protease inhibitors cocktail tablets (04693116001), and phosphatase inhibitor  
517 cocktail (04906837001) were from Roche Diagnostic (Mannheim, Germany). Camptothecin  
518 was purchased from Selleckchem (Munich, Germany).

519

520 *Antibodies*

521 The antibodies that were used in this study: mouse anti- $\beta$ -actin (AC-15, 1:20000) and mouse  
522 anti-FLAG (F-3165, 1:7000; IF 1:300) from Sigma-Aldrich; rabbit anti-TOP1 (A302-  
523 589A,1:5000), TOP2 $\alpha$  (A300-054A, 1:4000), TOP2 $\beta$  (A300-950A, 1:2000) and 53BP1(A300-  
524 272A,1:150) were from Bethyl Laboratories (Montgomery, Texas, USA); rabbit anti phospho-  
525 histone H2A.X clone 20E3 (#9718, IF:1:100) from Cell Signaling Technology (Danvers,  
526 Massachusetts); mouse monoclonal anti-ubiquitin (P4D1, sc-8017 1:1000), mouse anti-EBV-  
527 BZLF1 (sc-53904, 1:1000) and mouse anti-BRCA1 (D-9, sc-6954, IF 1:100) from Santa Cruz  
528 Biotechnology (Dallas, Texas, USA); mouse anti-SUMO2/3 (8A2, ab81371, 1:2000) from  
529 Abcam (Cambridge, MA, USA); monoclonal rat anti-EBV-BPLF1 (1:1500) (van Gent et al.,  
530 2014) from the MAB core facility, Helmholtz Center, Munich, Germany; mouse anti-EBV-  
531 BMRF1(1:10000) and rat anti-EBV-BFRF3 (1:1000) from Dr. Jaap M. Middeldorp (VU  
532 University Medical Center, Amsterdam, Netherlands). Alexa Fluor anti-rabbit-488 (A31570,  
533 1:1000) and anti-mouse-555 (A315721, 1:1000) conjugated secondary antibodies raised in  
534 donkey were from Thermo Fisher (Waltham, Massachusetts, USA).

535

536 *Plasmids and recombinant lentivirus vectors*

537 Eukaryotic expression vectors encoding the N-terminal domain of the EBV large tegument  
538 protein 3xFLAG-BPLF1 (amino acid 1-235) and the catalytic mutant BPLF1-C61A(Ascherio  
539 & Munger, 2015) and the bacterial expression vector His-BPLF1(Gupta et al., 2019) were  
540 described previously. Lentiviral vectors encoding N-terminal 3xFLAG and V5 tandem tagged  
541 versions of BPLF1 aa 1-325 and the corresponding catalytic mutant BPLF1-C61A under  
542 control of the doxycycline-inducible pTight promoter were produced by cloning the  
543 corresponding open reading frames(Ascherio & Munger, 2015) into a modified version of the  
544 pCW57.1 plasmid (gift from David Root, Addgene plasmid #41393). The Gal1/10 His6 TEV

545 Ura S. cerevisiae expression vector (12URA-B) was a gift from Scott Gradia (Addgene plasmid  
546 #48304) a plasmid expressing human TOP2 $\alpha$  was kindly provided by the James Berger (John  
547 Hopkins School of Medicine, Baltimore, USA). The FLAG-TOP2 $\alpha$  construct was created by  
548 in-frame cloning the 3xFLAG coding sequence (amino acids  
549 DYKDHDG DYKDHDIDYKDDDKL) at the N-terminus of the TOP2 $\alpha$  open reading frame.  
550 All cloning was performed using the ligation independent cloning protocol from the QB3  
551 Macrolab at Berkeley (macrolab.qb3.berkeley.edu). A recombinant lentivirus vector expressing  
552 the coding sequence of the EBV transactivator BZLF1 under control of a tetracycline-regulated  
553 promoter was constructed by cloning the open reading frame amplified with the primers 5'-  
554 CGACCGGTATGATGGACCCAACTCGAC-3' and 5'- CGACGCGTTAGAAATTAA  
555 GAGATCCTCGTGT-3' into the Age I and Mlu I sites of the pTRIPZ lentiviral vector (Thermo  
556 Fisher Scientific, USA). For virus production, HEK293FT cells were co-transfected with the  
557 pTRIPZ-BZLF1, psPAX and pMD2G plasmids (Addgene, Cambridge, MA) using JetPEI  
558 (Polyplus, Illkirch, France) according to the manufacture's protocol and cultured overnight in  
559 complete medium. After refreshing the medium, the cells were cultured for additional 48 h to  
560 allow virus production. Virus containing culture supernatant was briefly centrifuged and passed  
561 through a 0.45  $\mu$ m filter to removed cell debris before aliquoting and storing at -80°C for future  
562 use.

563

564 *Cell lines and transfection*

565 HeLa cells (ATCC RR-B51S) and HEK293T (ATCC CRL3216) cell lines were cultured in  
566 Dulbecco's minimal essential medium (DMEM, Sigma-Aldrich), supplemented with 10% FBS  
567 (Gibco-Invitrogen) and 10  $\mu$ g/ml ciprofloxacin (17850, Sigma-Aldrich) and grown in a 37°C  
568 incubator with 5% CO<sub>2</sub>. Stable HEK-rtTA-BPLF1/BPLF1-C61A cell lines were produced by  
569 lentiviral transduction followed by selection in medium containing 2 $\mu$ g/puromycin for 2 weeks.

570 Expression of FLAG-BPLF1/BPLF1-C61A was induced by treatment with 1.5 µg/ml  
571 doxycycline and confirmed by anti-FLAG immunofluorescence and Western blot analysis.  
572 Clones expressing high levels of the transduced proteins were selected by limiting dilution.  
573 HeLa cells were transiently transfected with plasmids expressing FLAG-tagged version of  
574 BPLF1/BPLF1-C61A using the lipofectamine 2000 (Invitrogen, California, USA) or jetPEI®  
575 (Polyplus transfection, Illkirch FR) DNA transfection reagent according to the protocols  
576 recommended by the manufacturer.

577

578 *Production of EBV immortalized lymphoblastoid cell lines (LCLs)*

579 Peripheral blood mononuclear cells were purified from Buffy coats (Blood Bank, Karolinska  
580 University Hospital, Stockholm, Sweden) by Ficoll-Paque (Lymphoprep, Axis-shield PoC AS,  
581 Oslo, Norway) density gradient centrifugation, and B-cells were affinity-purified using CD19  
582 microbeads (MACS MicroBeads, Miltenyi Biotec, Bergisch Gladbach, Germany) resulting in  
583 >95% pure B-cell populations. Infectious EBV encoding wild type or catalytic mutant BPLF1  
584 were rescued for HEK293-EBV cells as previously described(Gupta et al., 2018). One million  
585 B-cells were incubated in 1 ml virus preparation for 1.5 h at 37°C, followed by the addition of  
586 fresh complete medium and incubation at 37°C in a 5% CO<sub>2</sub> incubator until immortalized LCLs  
587 were established. Sublines expressing a doxycycline-inducible BZLF1 transactivator were  
588 produced by culturing 10<sup>6</sup> LCL cells with the recombinant lentivirus in presence of 8 µg/ml  
589 polybrene (TR-1003-G, Sigma-Aldrich) for 24 hours followed by replacement of the infection  
590 medium with fresh complete medium. The transduced cells were selected in medium containing  
591 0.8µg/ml (LCL-BPLF1) or 0.25µg/ml (LCL-BPLF1-C61A) puromycin for one or two weeks.

592

593 *Immunofluorescence*

594 Transfected HeLa and HEK-Tta-BPLF1/BPLF1-C61A cells were grown on coverslips and  
595 induced with 1.5 µg/ml doxycycline for 24 h. For immunofluorescence analysis, the cells were  
596 fixed with 4% formaldehyde for 20 min, followed by permeabilization with 0.05% Triton X-  
597 100 in PBS for 5 min and blocking in PBS containing 4% bovine serum albumin for 40 min.  
598 After incubation for 1 h with primary antibodies and washing 3x5 min in PBS, the cells were  
599 incubated for 1 h with the appropriate Alexa Fluor-conjugated secondary antibodies, followed  
600 by washing and mounting in Vectashield-containing DAPI (Vector Laboratories, Inc.  
601 Burlingame, CA, USA). Images were acquired using a fluorescence microscope (Leica DM  
602 RA2, Leica Microsystems, Wetzlar, Germany) equipped with a CCD camera (C4742-95,  
603 Hamamatsu, Japan). Fluorescence intensity was quantified using the ImageJ® software.

604

605 *Western blots*

606 Cells were lysed in RIPA buffer (25 mM Tris•HCl pH 7.6, 150 mM NaCl, 1% Igepal, 1%  
607 sodium deoxycholate, 2% SDS) supplemented with protease inhibitor cocktail. Loading buffer  
608 (Invitrogen) was added to each sample followed by boiling for 10 min at 100°C. The lysates  
609 were fractionated in acrylamide Bis-Tris 4-12% gradient gel (Life Technologies Corporation,  
610 Carlsbad, USA). After transfer to PVDF membranes (Millipore Corporation, Billerica, MA,  
611 USA), the blots were blocked in TBS (VWR, Radnor, Pennsylvania, USA) containing 0.1%  
612 Tween-20 and 5% non-fat milk, and the membranes were incubated with the primary antibodies  
613 diluted in blocking buffer for 1 h at room temperature or over-night at 4°C followed by washing  
614 and incubation for 1 h with the appropriate horseradish peroxidase-conjugated secondary  
615 antibodies. The immunocomplexes were visualized by enhanced chemiluminescence (GE  
616 Healthcare AB, Uppsala, SE). For detecting topoisomerase-DNA adducts after treatment with  
617 topoisomerase poisons, the cells were lysed in alkaline buffer(Ban et al., 2013). Briefly, cells  
618 treated for the indicated time with 5 µM Camptothecine or 80 µM Etoposide were lysed in

619 100  $\mu$ l in buffer containing 200 mM NaOH, 2 mM EDTA, followed by the addition of 100  $\mu$ l  
620 of 1M HEPES buffer (pH 7.4). Nucleic acids were removed by addition of 10  $\mu$ l 100 mM  
621 CaCl<sub>2</sub>, 2  $\mu$ l 1M DTT, and 200U of micrococcal nuclease followed by incubation at 37°C for  
622 20 min. Seventy  $\mu$ l of 4xLDS loading buffer (Invitrogen) were added to each sample followed  
623 by boiling for 10 min at 100°C before SDS-PAGE fractionation and western blot analysis.

624

625 *Immunoprecipitation and pull-down assays*

626 Cells were harvested 48h after transfection and lysed in NP40 lysis buffer (150 mM NaCl, 50  
627 mM Tris-HCl pH7.6, 5mM MgCl<sub>2</sub>, 1mM EDTA, 1% Igepal, 1 mM DTT, 10% glycerol)  
628 supplemented with protease/phosphatase inhibitor cocktail, 20 mM NEM and 20 mM  
629 Iodoacetamide for 30 min on ice. For immunoprecipitations under denaturing condition the  
630 lysis buffer was supplemented with 1% SDS followed by dilution to 0.1% SDS. For  
631 BPLF1/BPLF1-C61A co-immunoprecipitation, the lysates were incubated for 3 h with 50  $\mu$ l  
632 anti-FLAG packed agarose affinity gel (A-2220; Sigma) at 4 °C with rotation. After washing  
633 4 times with lysis buffer, the immunocomplexes were eluted with FLAG peptide (F4799;  
634 Sigma). For TOP2 $\alpha$  and TOP2 $\beta$  immunoprecipitation, specific antibodies were added to cell  
635 lysates and incubated at 4°C for 3 h with rotation. The protein-antibody complexes were  
636 captured with protein-G coupled Sepharose beads (GE Healthcare) by incubation at 4 °C for 1  
637 h. The beads were washed 4 times with lysis buffer followed by boiling in 2xSDS-PAGE  
638 loading for 10 min at 100°C. The production of 6xHis-BPLF1 in bacteria and purification of  
639 the recombinant protein were done as previously described(Gupta et al., 2019). Recombinant  
640 human TOP2 $\alpha$  was expressed and purified according to a previously published protocol with  
641 slight modifications(Lee et al., 2017). Briefly, URA-deficient yeast (kindly provided by Lena  
642 Ström, CMB Karolinska Institutet) were transformed with the TOP2 $\alpha$  expression plasmid,  
643 grown initially in uracil-deficient media, then in YPLG (1% yeast extract, 2% peptone, 2%

644 sodium DL-lactate, 1.5% glycerol) before induction of expression by addition of 2% galactose.  
645 The yeast was harvested by centrifugation and snap-frozen in liquid nitrogen. Proteins were  
646 extracted using a cryo-mill, and the filtered lysate was passed sequentially through HisTrap  
647 Excel nickel and HiTrap CP cation exchange columns (GE Healthcare) to purify the tagged  
648 TOP2 $\alpha$  protein before incubation overnight with His-tagged TEV protease. The following day,  
649 the protein was passed through a HisTrap column to remove the cleaved His-tag and the TEV  
650 protease. The TOP2 $\alpha$  protein was further purified on a Superdex 200 16/60 column,  
651 concentrated, and stored at -80°C. Relaxation and decatenation assays along with western  
652 blotting were performed to confirm protein purity and activity. Equimolar concentration of  
653 purified His-BPLF1 (0.35  $\mu$ g) and FLAG-TOP2 $\alpha$  (2  $\mu$ g) were incubated in binding buffer (100  
654 mM NaCl, 50 mM Tris-HCl, 1mM DTT, 0.5% Igepal) for 20 min at 4°C. Anti-FLAG agarose  
655 affinity gel (A-2220; Sigma) or Ni-NTA beads (Qiagen) were added followed by incubation  
656 for 60 min or 20 min at 4°C with rotation. The beads were intensively washed, and bound  
657 proteins were eluted with FLAG peptide or 300 mM imidazole in buffer containing 50 mM  
658 Tris-HCl pH 7.6, 50 mM NaCl and 1 mM DTT.

659

660 *Rapid approach to DNA adduct recovery (RADAR) assay*

661 TOP2ccs were isolated by RADAR assays as described(Kiianitsa & Maizels, 2013). Briefly,  
662 cells cultured in 6 well plates were treated with 80  $\mu$ M etoposide for 30 min or 4 h and then  
663 lysed in 800  $\mu$ l DNAzol. Following the addition of 400  $\mu$ l absolute ethanol, the lysates were  
664 cooled at -20°C and then centrifuged at 14000 rpm for 20 min at 4°C. After repeated washing  
665 in 75% ethanol the nucleic acid pellets were dissolved in 100  $\mu$ l H<sub>2</sub>O at 37°C for 15 minutes,  
666 followed by treatment with 100  $\mu$ g/ml RNaseA. The concentration of DNA was measured and  
667 10  $\mu$ g DNA from each sample were treated with 250 U micrococcal nuclease supplemented

668 with 5 mM CaCl<sub>2</sub> before the addition of loading buffer and detection of trapped protein by  
669 western blot.

670

671 *Reverse transcription and real-time PCR*

672 Total RNA was isolated using the Quick-RNA MiniPrep kit (Zymo Research, Irvine, CA, USA)  
673 with in-column DNase treatment according to the instructions of the manufacturer. One  
674 microgram of total RNA was reverse transcribed using SuperScript VILO cDNA Synthesis kit  
675 (Invitrogen). PCR amplification was performed with the LC FastStart DNA master SYBR green  
676 I kit in a LightCycler 1.2 instrument (Roche Diagnostic) using the following specific primers:  
677 TOP1 5'-AGTGGAAAGAAGTCCGGCATGA-3', 5'-GCCAGTCCTCTCACCCCT TGAT-  
678 3'; TOP2 $\alpha$  5'-AAGCCCAGCAAAAGGTTCCA-3', 5'-TGGCTTCAACAGCCTCCA AT-3';  
679 TOP2 $\beta$  5'-GGTCGTGTAGAGGGGTCAA-3', 5'-CCCAGTTCATCCAATTGT C-3';  
680 BPLF1 5'-CATACACCGTGCAGAAAGAA-3', 5'-GATGGCGGGTAATACATGCT-3'; and  
681 MLN51 (Metastatic Lymph Node 51) 5'-CAAGGAAGGTCGTGCTGGTT-3', 5'-AC  
682 CAGACCGGCCACCAT-3' as endogenous control gene. The PCR reactions were denatured at  
683 95°C for 10 min, followed by 40 cycles at 95°C for 8 sec, 60°C for 5 sec, 72°C for 8 sec. The  
684 relative levels of mRNA were determined from the standard curve using MLN51 as reference.

685

686 *MTT assay*

687 For assay of cell viability, 2 $\times$ 10<sup>4</sup> HEK-rtTABPLF1/BPLF1-C61A or 5 $\times$ 10<sup>4</sup> LCLEBV-  
688 BPLF1/BPLF1-C61A were plated in 150  $\mu$ l medium in triplicate wells of a 96 well plate  
689 without or with the addition of the indicated concentrations of Etoposide. After incubation for  
690 20 h at 37°C in a 5% CO<sub>2</sub> incubator, 50  $\mu$ l culture medium containing 1 mg/ml  
691 Methylthiazolyldiphenyl-tetrazolium bromide (MTT, M5655, Sigma-Aldrich) were added to

692 the wells followed by incubation for additional 4 h. The MTT formazan crystals produced by  
693 mitochondrial dehydrogenases in living cells were solubilized by the addition of 50 µl 10%  
694 SDS and O.D. was measured at 540 nm in a plate reader. Relative viability was calculated after  
695 subtraction of the background O.D. of media alone.

696

697 *EBV DNA replication and release of infectious virus*

698 Virus replication and the release of infectious virus were monitored after induction with 1.5  
699 µg/ml Doxycycline for 3 days in cell pellets and culture supernatants by quantitative PCR.  
700 Briefly, DNA was isolated from cell pellets and culture supernatants cleared of cell debris by  
701 centrifugation of 5 min at 14000 rpm and treated with 20 U/ml DNase I (Promega, Madison,  
702 WI, USA) to remove free viral DNA, using the DNeasy Blood & Tissue Kit (Qiagen, Hilden,  
703 Germany). Quantitative PCR was performed Quantitative PCR was performed as described  
704 above with primers specific for a unique sequence in EBNA1 5'- GGCAGTGGACCTCAAAG  
705 AAG-3', 5'-CTATGTCTTGGCCCTGATCC-3' and the cellular EF1 $\alpha$  (Elongation  
706 factor 1 $\alpha$ ) 5'-CTGAACCATCCAGGCCAAAT-3', 5'-GCCGTGTGGCAATCCAAT-3' as  
707 reference. Virus replication was calculated as the ratio between the amount of viral DNA in  
708 induced versus untreated cells.

709

710

711 **REFERENCES**

712 Anand, J., Sun, Y., Zhao, Y., Nitiss, K. C., & Nitiss, J. L. (2018). Detection of Topoisomerase  
713 Covalent Complexes in Eukaryotic Cells. *Methods Mol Biol*, 1703, 283-299.  
714 [https://doi.org/10.1007/978-1-4939-7459-7\\_20](https://doi.org/10.1007/978-1-4939-7459-7_20)

715

716 Ascherio, A., & Munger, K. L. (2015). EBV and Autoimmunity. *Curr Top Microbiol Immunol*,  
717 390(Pt 1), 365-385. [https://doi.org/10.1007/978-3-319-22822-8\\_15](https://doi.org/10.1007/978-3-319-22822-8_15)

718

719 Babcock, G. J., Decker, L. L., Volk, M., & Thorley-Lawson, D. A. (1998, Sep). EBV persistence in  
720 memory B cells in vivo. *Immunity*, 9(3), 395-404. [https://doi.org/10.1016/s1074-7613\(00\)80622-6](https://doi.org/10.1016/s1074-7613(00)80622-6)

721

722

723 Bailey-Elkin, B. A., Knaap, R. C. M., Kikkert, M., & Mark, B. L. (2017, Nov 10). Structure and  
724 Function of Viral Deubiquitinating Enzymes. *J Mol Biol*, 429(22), 3441-3470.  
725 <https://doi.org/10.1016/j.jmb.2017.06.010>

726

727 Ban, Y., Ho, C. W., Lin, R. K., Lyu, Y. L., & Liu, L. F. (2013, Oct). Activation of a novel ubiquitin-  
728 independent proteasome pathway when RNA polymerase II encounters a protein  
729 roadblock. *Mol Cell Biol*, 33(20), 4008-4016. <https://doi.org/10.1128/MCB.00403-13>

730

731 Benson, J. D., & Huang, E. S. (1988, Dec). Two specific topoisomerase II inhibitors prevent  
732 replication of human cytomegalovirus DNA: an implied role in replication of the viral  
733 genome. *J Virol*, 62(12), 4797-4800. <https://doi.org/10.1128/JVI.62.12.4797-4800.1988>

732

733

734

735

736 Benson, J. D., & Huang, E. S. (1990, Jan). Human cytomegalovirus induces expression of cellular  
737 topoisomerase II. *J Virol*, 64(1), 9-15. <https://doi.org/10.1128/JVI.64.1.9-15.1990>

737

738

739 Borgermann, N., Ackermann, L., Schwertman, P., Hendriks, I. A., Thijssen, K., Liu, J. C., Lans, H.,  
740 Nielsen, M. L., & Mailand, N. (2019, Apr 15). SUMOylation promotes protective  
741 responses to DNA-protein crosslinks. *EMBO J*, 38(8).  
742 <https://doi.org/10.15252/embj.2019101496>

743

744 Borozan, I., Zapatka, M., Frappier, L., & Ferretti, V. (2018, Jan 15). Analysis of Epstein-Barr  
745 Virus Genomes and Expression Profiles in Gastric Adenocarcinoma. *J Virol*, 92(2).  
746 <https://doi.org/10.1128/JVI.01239-17>

747

748 Champoux, J. J. (2001). DNA topoisomerases: structure, function, and mechanism. *Annu Rev  
749 Biochem*, 70, 369-413. <https://doi.org/10.1146/annurev.biochem.70.1.369>

750

751 Chen, T., Sun, Y., Ji, P., Kopetz, S., & Zhang, W. (2015, Jul 30). Topoisomerase IIalpha in  
752 chromosome instability and personalized cancer therapy. *Oncogene*, 34(31), 4019-  
753 4031. <https://doi.org/10.1038/onc.2014.332>

754

755 Countryman, J., & Miller, G. (1985, Jun). Activation of expression of latent Epstein-Barr  
756 herpesvirus after gene transfer with a small cloned subfragment of heterogeneous  
757 viral DNA. *Proc Natl Acad Sci U S A*, 82(12), 4085-4089.  
758 <https://doi.org/10.1073/pnas.82.12.4085>  
759

760 Delgado, J. L., Hsieh, C. M., Chan, N. L., & Hiasa, H. (2018, Jan 23). Topoisomerase as  
761 anticancer targets. *Biochem J*, 475(2), 373-398. <https://doi.org/10.1042/BCJ20160583>  
762

763 Ebert, S. N., Shtrom, S. S., & Muller, M. T. (1990, Sep). Topoisomerase II cleavage of herpes  
764 simplex virus type 1 DNA in vivo is replication dependent. *J Virol*, 64(9), 4059-4066.  
765 <https://doi.org/10.1128/JVI.64.9.4059-4066.1990>  
766

767 Feederle, R., Kost, M., Baumann, M., Janz, A., Drouet, E., Hammerschmidt, W., & Delecluse, H.  
768 J. (2000, Jun 15). The Epstein-Barr virus lytic program is controlled by the co-operative  
769 functions of two transactivators. *EMBO J*, 19(12), 3080-3089.  
770 <https://doi.org/10.1093/emboj/19.12.3080>  
771

772 Gao, R., Schellenberg, M. J., Huang, S. Y., Abdelmalak, M., Marchand, C., Nitiss, K. C., Nitiss, J.  
773 L., Williams, R. S., & Pommier, Y. (2014, Jun 27). Proteolytic degradation of  
774 topoisomerase II (Top2) enables the processing of Top2.DNA and Top2.RNA covalent  
775 complexes by tyrosyl-DNA-phosphodiesterase 2 (TDP2). *J Biol Chem*, 289(26), 17960-  
776 17969. <https://doi.org/10.1074/jbc.M114.565374>  
777

778 Gastaldello, S., Chen, X., Callegari, S., & Masucci, M. G. (2013). Caspase-1 promotes Epstein-  
779 Barr virus replication by targeting the large tegument protein deneddylase to the  
780 nucleus of productively infected cells. *PLoS Pathog*, 9(10), e1003664.  
781 <https://doi.org/10.1371/journal.ppat.1003664>  
782

783 Gastaldello, S., Hildebrand, S., Faridani, O., Callegari, S., Palmkvist, M., Di Guglielmo, C., &  
784 Masucci, M. G. (2010, Apr). A deneddylase encoded by Epstein-Barr virus promotes  
785 viral DNA replication by regulating the activity of cullin-RING ligases. *Nat Cell Biol*,  
786 12(4), 351-361. <https://doi.org/10.1038/ncb2035>  
787

788 Gomez-Herreros, F., Romero-Granados, R., Zeng, Z., Alvarez-Quilon, A., Quintero, C., Ju, L.,  
789 Umans, L., Vermeire, L., Huylebroeck, D., Caldecott, K. W., & Cortes-Ledesma, F.  
790 (2013). TDP2-dependent non-homologous end-joining protects against topoisomerase  
791 II-induced DNA breaks and genome instability in cells and in vivo. *PLoS Genet*, 9(3),  
792 e1003226. <https://doi.org/10.1371/journal.pgen.1003226>  
793

794 Gomez-Herreros, F., Zagnoli-Vieira, G., Ntai, I., Martinez-Macias, M. I., Anderson, R. M.,  
795 Herrero-Ruiz, A., & Caldecott, K. W. (2017, Aug 10). TDP2 suppresses chromosomal  
796 translocations induced by DNA topoisomerase II during gene transcription. *Nat  
797 Commun*, 8(1), 233. <https://doi.org/10.1038/s41467-017-00307-y>  
798

799 Gupta, S., Yla-Anttila, P., Callegari, S., Tsai, M. H., Delecluse, H. J., & Masucci, M. G. (2018, Jan).  
800 Herpesvirus deconjugases inhibit the IFN response by promoting TRIM25

autoubiquitination and functional inactivation of the RIG-I signalosome. *PLoS Pathog*, 14(1), e1006852. <https://doi.org/10.1371/journal.ppat.1006852>

Gupta, S., Yla-Anttila, P., Sandalova, T., Sun, R., Achour, A., & Masucci, M. G. (2019, Nov). 14-3-3 scaffold proteins mediate the inactivation of trim25 and inhibition of the type I interferon response by herpesvirus deconjugases. *PLoS Pathog*, 15(11), e1008146. <https://doi.org/10.1371/journal.ppat.1008146>

Hammarsten, O., Yao, X., & Elias, P. (1996, Jul). Inhibition of topoisomerase II by ICRF-193 prevents efficient replication of herpes simplex virus type 1. *J Virol*, 70(7), 4523-4529. <https://www.ncbi.nlm.nih.gov/pubmed/8676478>

Hammerschmidt, W., & Sugden, B. (2013, Jan 1). Replication of Epstein-Barr viral DNA. *Cold Spring Harb Perspect Biol*, 5(1), a013029. <https://doi.org/10.1101/cshperspect.a013029>

Hoa, N. N., Shimizu, T., Zhou, Z. W., Wang, Z. Q., Deshpande, R. A., Paull, T. T., Akter, S., Tsuda, M., Furuta, R., Tsutsui, K., Takeda, S., & Sasanuma, H. (2016, Nov 3). Mre11 Is Essential for the Removal of Lethal Topoisomerase 2 Covalent Cleavage Complexes. *Mol Cell*, 64(3), 580-592. <https://doi.org/10.1016/j.molcel.2016.10.011>

Kattenhorn, L. M., Korbel, G. A., Kessler, B. M., Spooner, E., & Ploegh, H. L. (2005, Aug 19). A deubiquitinating enzyme encoded by HSV-1 belongs to a family of cysteine proteases that is conserved across the family Herpesviridae. *Mol Cell*, 19(4), 547-557. <https://doi.org/10.1016/j.molcel.2005.07.003>

Kaufmann, S. H. (1998, Oct 1). Cell death induced by topoisomerase-targeted drugs: more questions than answers. *Biochim Biophys Acta*, 1400(1-3), 195-211. [https://doi.org/10.1016/s0167-4781\(98\)00136-5](https://doi.org/10.1016/s0167-4781(98)00136-5)

Kawanishi, M. (1993, Oct). Topoisomerase I and II activities are required for Epstein-Barr virus replication. *J Gen Virol*, 74 ( Pt 10), 2263-2268. <https://doi.org/10.1099/0022-1317-74-10-2263>

Kawanishi, M. (1993). Topoisomerase I and II are required for Epstein-Barr virus replication. *J Gen Virol*, 74, 2263-2269. <https://doi.org/10.1099/0022-1317-74-10-2263>

Kianitsa, K., & Maizels, N. (2013, May). A rapid and sensitive assay for DNA-protein covalent complexes in living cells. *Nucleic Acids Res*, 41(9), e104. <https://doi.org/10.1093/nar/gkt171>

Komander, D. (2009, Oct). The emerging complexity of protein ubiquitination. *Biochem Soc Trans*, 37(Pt 5), 937-953. <https://doi.org/10.1042/BST0370937>

Kudoh, A., Fujita, M., Kiyono, T., Kuzushima, K., Sugaya, Y., Izuta, S., Nishiyama, Y., & Tsurumi, T. (2003, Jan). Reactivation of lytic replication from B cells latently infected with Epstein-Barr virus occurs with high S-phase cyclin-dependent kinase activity while

848 inhibiting cellular DNA replication. *J Virol*, 77(2), 851-861.  
849 <https://doi.org/10.1128/jvi.77.2.851-861.2003>

850

851 Lee, J. H., Wendorff, T. J., & Berger, J. M. (2017, Dec 22). Resveratrol: A novel type of  
852 topoisomerase II inhibitor. *Journal of Biological Chemistry*, 292(51), 21011-21022.  
853 <https://doi.org/10.1074/jbc.M117.810580>

854

855 Lee, K. C., Bramley, R. L., Cowell, I. G., Jackson, G. H., & Austin, C. A. (2016, Mar 1). Proteasomal  
856 inhibition potentiates drugs targeting DNA topoisomerase II. *Biochem Pharmacol*, 103,  
857 29-39. <https://doi.org/10.1016/j.bcp.2015.12.015>

858

859 Li, J., Callegari, S., & Masucci, M. G. (2017, Apr). The Epstein-Barr virus miR-BHRF1-1 targets  
860 RNF4 during productive infection to promote the accumulation of SUMO conjugates  
861 and the release of infectious virus. *PLoS Pathog*, 13(4), e1006338.  
862 <https://doi.org/10.1371/journal.ppat.1006338>

863

864 Lopez-Mosqueda, J., Maddi, K., Prgomet, S., Kalayil, S., Marinovic-Terzic, I., Terzic, J., & Dikic,  
865 I. (2016, Nov 17). SPRTN is a mammalian DNA-binding metalloprotease that resolves  
866 DNA-protein crosslinks. *eLife*, 5. <https://doi.org/10.7554/eLife.21491>

867

868 Madabhushi, R. (2018, Jun 29). The Roles of DNA Topoisomerase IIbeta in Transcription. *Int J  
869 Mol Sci*, 19(7). <https://doi.org/10.3390/ijms19071917>

870

871 Mah, L. J., El-Osta, A., & Karagiannis, T. C. (2010, Apr). gammaH2AX: a sensitive molecular  
872 marker of DNA damage and repair. *Leukemia*, 24(4), 679-686.  
873 <https://doi.org/10.1038/leu.2010.6>

874

875 Mao, Y., Desai, S. D., Ting, C. Y., Hwang, J., & Liu, L. F. (2001, Nov 2). 26 S proteasome-mediated  
876 degradation of topoisomerase II cleavable complexes. *J Biol Chem*, 276(44), 40652-  
877 40658. <https://doi.org/10.1074/jbc.M104009200>

878

879 McKinnon, P. J. (2016, Nov). Topoisomerases and the regulation of neural function. *Nat Rev  
880 Neurosci*, 17(11), 673-679. <https://doi.org/10.1038/nrn.2016.101>

881

882 Morimoto, S., Tsuda, M., Bunch, H., Sasanuma, H., Austin, C., & Takeda, S. (2019, Oct 30). Type  
883 II DNA Topoisomerases Cause Spontaneous Double-Strand Breaks in Genomic DNA.  
884 *Genes (Basel)*, 10(11). <https://doi.org/10.3390/genes10110868>

885

886 Munz, C. (2019, Nov). Latency and lytic replication in Epstein-Barr virus-associated  
887 oncogenesis. *Nat Rev Microbiol*, 17(11), 691-700. [https://doi.org/10.1038/s41579-019-0249-7](https://doi.org/10.1038/s41579-<br/>888 019-0249-7)

889

890 Murata, T. (2014, Jun). Regulation of Epstein-Barr virus reactivation from latency. *Microbiol  
891 Immunol*, 58(6), 307-317. <https://doi.org/10.1111/1348-0421.12155>

892

893 Nimonkar, A. V., & Boehmer, P. E. (2004, May 21). Role of protein-protein interactions during  
894 herpes simplex virus type 1 recombination-dependent replication. *J Biol Chem*,  
895 279(21), 21957-21965. <https://doi.org/10.1074/jbc.M400832200>

896

897 Nitiss, J. L. (2009, May). DNA topoisomerase II and its growing repertoire of biological  
898 functions. *Nat Rev Cancer*, 9(5), 327-337. <https://doi.org/10.1038/nrc2608>

899

900 Peng, R. J., Han, B. W., Cai, Q. Q., Zuo, X. Y., Xia, T., Chen, J. R., Feng, L. N., Lim, J. Q., Chen, S.  
901 W., Zeng, M. S., Guo, Y. M., Li, B., Xia, X. J., Xia, Y., Laurensia, Y., Chia, B. K. H., Huang,  
902 H. Q., Young, K. H., Lim, S. T., Ong, C. K., Zeng, Y. X., & Bei, J. X. (2019, Jun). Genomic  
903 and transcriptomic landscapes of Epstein-Barr virus in extranodal natural killer T-cell  
904 lymphoma. *Leukemia*, 33(6), 1451-1462. <https://doi.org/10.1038/s41375-018-0324-5>

905

906 Perry, M., Sundeep Kollala, S., Beigert, M., Su, G., Kodavati, M., Mallard, H., Kreling, N.,  
907 Holfrook, A., & Ghosal, G. (2020). USP11 deubiquitinates monoubiquitinated SPRTN to  
908 repair DNA-protein crosslinks. *bioRxiv*, <https://doi.org/10.1101/2020.06.30.180471>.

909

910 Pommier, Y. (2013, Jan 18). Drugging topoisomerase: lessons and challenges. *ACS Chem Biol*,  
911 8(1), 82-95. <https://doi.org/10.1021/cb300648v>

912

913 Pommier, Y., Huang, S. Y., Gao, R., Das, B. B., Murai, J., & Marchand, C. (2014, Jul). Tyrosyl-  
914 DNA-phosphodiesterases (TDP1 and TDP2). *DNA Repair (Amst)*, 19, 114-129.  
915 <https://doi.org/10.1016/j.dnarep.2014.03.020>

916

917 Povirk, L. F. (1996, Aug 17). DNA damage and mutagenesis by radiomimetic DNA-cleaving  
918 agents: bleomycin, neocarzinostatin and other enediynes. *Mutat Res*, 355(1-2), 71-89.  
919 [https://doi.org/10.1016/0027-5107\(96\)00023-1](https://doi.org/10.1016/0027-5107(96)00023-1)

920

921 Schellenberg, M. J., Lieberman, J. A., Herrero-Ruiz, A., Butler, L. R., Williams, J. G., Munoz-  
922 Cabello, A. M., Mueller, G. A., London, R. E., Cortes-Ledesma, F., & Williams, R. S. (2017,  
923 Sep 29). ZATT (ZNF451)-mediated resolution of topoisomerase 2 DNA-protein cross-  
924 links. *Science*, 357(6358), 1412-1416. <https://doi.org/10.1126/science.aam6468>

925

926 Sciascia, N., Wu, W., Zong, D., Sun, Y., Wong, N., John, S., Wangsa, D., Ried, T., Bunting, S. F.,  
927 Pommier, Y., & Nussenzweig, A. (2020, Feb 14). Suppressing proteasome mediated  
928 processing of topoisomerase II DNA-protein complexes preserves genome integrity.  
929 *Elife*, 9. <https://doi.org/10.7554/elife.53447>

930

931 Shannon-Lowe, C., & Rickinson, A. (2019). The Global Landscape of EBV-Associated Tumors.  
932 *Front Oncol*, 9, 713. <https://doi.org/10.3389/fonc.2019.00713>

933

934 Stingele, J., Bellelli, R., Alte, F., Hewitt, G., Sarek, G., Maslen, S. L., Tsutakawa, S. E., Borg, A.,  
935 Kjaer, S., Tainer, J. A., Skehel, J. M., Groll, M., & Boulton, S. J. (2016, Nov 17).  
936 Mechanism and Regulation of DNA-Protein Crosslink Repair by the DNA-Dependent  
937 Metalloprotease SPRTN. *Mol Cell*, 64(4), 688-703.  
938 <https://doi.org/10.1016/j.molcel.2016.09.031>

939

940 Sun, Y., Miller Jenkins, L. M., Su, Y. P., Nitiss, K. C., Nitiss, J. L., & Pommier, Y. (2020, Nov). A  
941 conserved SUMO pathway repairs topoisomerase DNA-protein cross-links by engaging  
942 ubiquitin-mediated proteasomal degradation. *Sci Adv*, 6(46).  
943 <https://doi.org/10.1126/sciadv.aba6290>  
944

945 Sun, Y., Saha, L. K., Saha, S., Jo, U., & Pommier, Y. (2020, Oct). Debulking of topoisomerase  
946 DNA-protein crosslinks (TOP-DPC) by the proteasome, non-proteasomal and non-  
947 proteolytic pathways. *DNA Repair (Amst)*, 94, 102926.  
948 <https://doi.org/10.1016/j.dnarep.2020.102926>  
949

950 van Gent, M., Braem, S. G., de Jong, A., Delagic, N., Peeters, J. G., Boer, I. G., Moynagh, P. N.,  
951 Kremmer, E., Wiertz, E. J., Ovaa, H., Griffin, B. D., & Ressing, M. E. (2014, Feb). Epstein-  
952 Barr virus large tegument protein BPLF1 contributes to innate immune evasion  
953 through interference with toll-like receptor signaling. *PLoS Pathog*, 10(2), e1003960.  
954 <https://doi.org/10.1371/journal.ppat.1003960>  
955

956 Wang, J. C. (2002, Jun). Cellular roles of DNA topoisomerases: a molecular perspective. *Nat  
957 Rev Mol Cell Biol*, 3(6), 430-440. <https://doi.org/10.1038/nrm831>  
958

959 Wang, P., Rennekamp, A. J., Yuan, Y., & Lieberman, P. M. (2009, Aug). Topoisomerase I and  
960 RecQL1 function in Epstein-Barr virus lytic reactivation. *J Virol*, 83(16), 8090-8098.  
961 <https://doi.org/10.1128/JVI.02379-08>  
962

963 Wang, Y., Li, H., Tang, Q., Maul, G. G., & Yuan, Y. (2008, Mar). Kaposi's sarcoma-associated  
964 herpesvirus ori-Lyt-dependent DNA replication: involvement of host cellular factors. *J  
965 Virol*, 82(6), 2867-2882. <https://doi.org/10.1128/JVI.01319-07>  
966

967